ELSEVIER

Ultramicroscopy 65 (1996) 101–107

ultramicroscopy

Comparison of calculated and observed dynamical diffraction from purple membrane: implications

N. Grigorieff *, R. Henderson

MRC Laboratory of Molecular Biology, Hills Road, Cambridge CB2 2QH, UK

Received 3 May 1996; accepted 16 July 1996

Abstract

We show that the magnitude and direction of the observed differences in intensities of Friedel-related reflections in electron diffraction patterns from two-dimensional crystals of bacteriorhodopsin (purple membrane) are accounted for by dynamical scattering as well as by Ewald sphere curvature. We suggest how the observed Friedel differences might be used to refine structure factor phases.

Keywords: Electron diffraction; Elastic scattering theory

1. Introduction

Dynamical (multiple) diffraction of electrons in a transmission electron microscope is a consequence of the strong interaction between electrons and the sample. Depending on the sample thickness, diffraction amplitudes and phases may deviate significantly from their kinematical (single) diffraction values. Kinematical diffraction data, as normally obtained from X-ray diffraction experiments, are related to the density by means of a simple Fourier transform. A corresponding inverse mathematical operation for dynamical diffraction data does not exist as yet, and structural work is restricted either to simple structures where dynamical scattering may be strong, such as semiconductor crystals [1], or to weakly scattering samples (weak phase objects), such as two-dimensional protein crystals, which are thin with large unit cells. In the second case, kinematical diffraction theory can be applied to solve the structure in broad outline without the necessity to consider dynamical diffraction.

The membrane protein bacteriorhodopsin (bR) is the light-driven proton pump in halobacteria. Together with lipid molecules and the chromophore retinal, it forms two-dimensional crystals (purple membrane) which exist in vivo and are relatively easy to isolate. Diffraction patterns and images from untilted and tilted specimens have provided amplitudes and phases to yield a density map of near atomic resolution [2] which could be interpreted with an atomic model for the protein [3]. The analysis of the data assumed kinematical conditions. The very small deviation from kinematical conditions was verified by measurement of dynamical perturbations leading to differences in intensities of Friedel-related reflections in experimental diffraction patterns [4]. The average difference in Friedel-related intensities up to 7 Å was found to be 6.4% at 120 keV which is

* Corresponding author. Tel: +44-1223-402223; fax: +44-1223-213556; e-mail: niko@mrc-lmb.cam.ac.uk.

PII S0304-3991(96)00061-7

significantly higher than expected from the curvature of the Ewald sphere alone (about 1.6%), and this was attributed to dynamical diffraction. Furthermore, simulations on a computer showed that the average intensity of a Friedel pair in a dynamical diffraction pattern is an excellent approximation to its kinematical value [5] differing by less than 1%. Thus, the analysis of the data could proceed without problems.

Although reproducible differences in Friedel pairs were found in experimental diffraction patterns as well as in simulations, a correlation between the two sets of data to demonstrate conclusively that dynamical scattering accounts, in magnitude and direction, for the observed differences, has never been carried out. This is now done with diffraction data previously used to derive the model for bR [6], and with simulations based on the multi-slice method [7] to calculate dynamical diffraction intensities. We also relate the absolute scale of the diffraction amplitudes (in comparison to the direct, unscattered beam) with the magnitude of the dynamical differences. Finally, we show that the differences in Friedel pairs can be used in the refinement of structure factor phases.

2. Methods

The experimental electron diffraction data were obtained by Ceska and Henderson [6] from the p3 crystal form of bR (purple membrane), embedded in glucose by air-drying. The data were collected on Philips 400 and 420 electron microscopes operated at 120 kV and with the specimens cooled to −120°C. Diffraction intensities were measured on film using the procedure of Baldwin and Henderson [8].

The atomic model used in the calculation includes residues 7 to 227 out of a total of 248 residues for bR, the chromophore retinal and 10 phospholipids [3]. It was crystallographically refined to an *R*-factor of 28% and a phase residual of 58° against electron diffraction data corrected for diffuse background due to partial disorder in the crystals [9]. The experimental density map used in the work presented here has a resolution of 3.5 Å parallel and 4.3 Å perpendicular to the plane of the membrane [3].

For the calculation of dynamical diffraction intensities a program was written based on the multi-slice procedure [7,10]. The program takes either atomic coordinates from a protein databank (PDB) file together with a file of atomic scattering factors, or a density map representing the shielded Coulomb potential inside the sample. Diffraction intensities can be calculated that are fully dynamical, or kinematical including effects due to the curvature of the Ewald sphere. Absorption is an important factor in the accurate calculation of diffraction intensities and can cause differences in Friedel-related reflections [11]. However, the absorptive potential describing inelastic scattering is only a small fraction (typically 0.1 or less) of the elastic potential [12,13]. Therefore, we expect the errors in the calculation due to the missing absorptive terms to be small in comparison with the Friedel differences caused by elastic dynamical scattering, and we will ignore absorption here.

To compare two data sets a correlation coefficient r was calculated with

$$r = \frac{\sum_{i=1}^{n} \Delta I_i^e \Delta I_i^c}{\sqrt{\sum_{i=1}^{n} (\Delta I_i^e)^2 \sum_{i=1}^{n} (\Delta I_i^c)^2}} . \quad (1)$$

Here, ΔI_i^e and ΔI_i^c are the experimental and calculated intensity differences in Friedel pair i, n is the number of reflections compared, and the average over all Friedel differences was taken to be zero. Assuming a normal distribution for the experimental errors the significance of the deviation of r from zero can be tested by comparison to the standard deviation of r for uncorrelated data, with

$$\sigma_r \approx \frac{1 - r^2}{\sqrt{n}} . \quad (2)$$

In protein crystallography, an *R*-factor is usually calculated to test for agreement between sets of diffraction intensities. We will use it here to compare experimental and calculated intensities. It is defined as

$$R = \frac{\sum_{i=1}^{n} |\sqrt{I_i^e} - \sqrt{I_i^c}|}{\sum_{i=1}^{n} \sqrt{I_i^e}} . \quad (3)$$

I_i^e and I_i^c are the averages of experimental and calculated Friedel-related intensities.

Finally, the parameter b together with its standard deviation σ_b in a linear fit minimising

$$\sum_{i=1}^{n} \left(\Delta I_i^e - b \Delta I_i^c \right)^2 \quad (4)$$

was calculated relating the magnitude of experimental and calculated Friedel differences. This was done after scaling the experimental intensities I_i^e and Friedel differences ΔI_i^e to those calculated using a scale factor and a temperature factor derived by minimising the R-factor. If experimental and calculated Friedel differences are of the same magnitude we expect b to be close to 1.0.

Table 1
Correlation coefficients r and standard deviations σ_r (in parentheses) between Friedel differences observed in diffraction patterns from untilted (tilt angle smaller than 1.5°) samples at 3.5 Å. The self-correlation is done between symmetry-related reflection within each film. About 400 Friedel differences were included in each correlation coefficient

Film number	746	857	858
746	0.47	−0.43	−0.45
	(0.04)	(0.04)	(0.04)
857		0.45	0.53
		(0.04)	(0.04)
858			0.54
			(0.04)

3. Results and discussion

Before discussing the results in detail, the following preliminary considerations are important: (a) In the kinematical approximation inversion of the beam direction has no effect on the calculated intensities. This is no longer valid when dynamical scattering is taken into account. The correct orientation of the sample was determined from the diffraction pattern in each case. It was found, however, that a reversal of the beam direction in a calculation caused only small changes in the intensities, presumably because the extent of dynamical scattering is still relatively small. (b) The indexing of Friedel-related reflections may be reversed ($h \rightarrow -h$; $k \rightarrow -k$) between patterns since phases are not recorded and it is not possible to determine the sign of the reflection on each pattern prior to further analysis. Thus, positive as well as negative correlation coefficients are possible. (c) Dynamical scattering depends on the density (shielded Coulomb potential) of the sample. The absolute scale of the density can be determined by measuring the intensity of a diffracted beam relative to that of the transmitted beam. For the density scaling, reflection (4, 3, 0) was chosen because it is one of the strongest reflections. Its intensity was found to be 2.5×10^{-5} of that of the main beam. It is interesting to note that the density is also determined on an absolute scale by the form factors in calculations using the atomic model. The form factors used assume neutral, unbonded atoms and were taken from the International Tables for Crystallography [14]. However, at a resolution below about 2.5 Å, form factors are not accurately known and are sensitive to chemical bonding [12,15,16,3]. Comparison of the density scaled using the (4, 3, 0) reflection with the density calculated using the atomic model and tabulated form factors for neutral atoms [14] shows that the former is smaller by a factor of about 1.6. This could be due partly to an average shrinkage of orbitals due to bonding which would then increase the screening of the positively charged nuclei by the negatively charged electron clouds to give an overall smaller potential. It is also possible that the observed difference in scale between experimental density map and the map calculated from the model reflects small inaccuracies in the model.

Table 1 summarises correlation coefficients of Friedel differences in diffraction data from untilted specimens. The correlation of Friedel differences on two different films as well as the correlation of p3 symmetry-related reflections on the same film is much higher than the standard deviation σ_r expected for a correlation coefficient of uncorrelated data. This confirms the supposition that the observed Friedel differences are not due to random error in the measurement but represent a systematic effect.

Correlation coefficients between observed and calculated Friedel differences assuming kinematical or dynamical diffraction are given in Table 2 for untilted and tilted films, along with R-factors and ratios (coefficient b in the linear fit, see Section 2) of observed to calculated Friedel differences. When comparing calculated and observed data it was found that a higher correlation was obtained for a calcula-

tion using the experimental density map compared to a calculation using the refined atomic model. This is not surprising in view of the overall R-factor of 28% between the model and the experimental data and a phase residual of 58°. It indicates residual deficiencies in the atomic model. However, except for film 560, the correlation coefficients in each case are 10 to 20 times higher than their corresponding σ_r for uncorrelated data. Film 560 shows a significantly lower correlation with both types of dynamical calculation as well as with the kinematical calculation. The membrane giving rise to this diffraction pattern may not have been entirely flat, thus causing the diffraction data to consist of a slight mixture of different patterns. The clear correspondence of the observed data with the calculation is illustrated in Fig. 1 where all the observed and calculated Friedel differences are plotted for a particular diffraction pattern. A line representing a linear fit to the data (see Section 2) is also shown and has a slope of 0.91 (cf. Table 2). The expected slope of the line would be 1.0. The small deviation found here may be due to both the experimental error in the measured data and an inaccuracy in the relative scaling of the experimental and calculated data. The plot shows that the distribution of data points is anisotropic and has a spread which is wider along the line than perpendicular to it. Smaller Friedel differences near the origin of the plot show weaker correlation (more isotropic distribution) as other effects (e.g. absorption, Ewald sphere curvature, error in the measurements) dominate. The average ratio (coefficient b in the linear fit) of observed to calculated Friedel differences when using the map is close to 1.0 for most films analysed (cf. Table 2), thus confirming the density scaling found earlier using the intensity of the (4, 3, 0) reflection. The ratios found in calculations using the atomic model were generally lower.

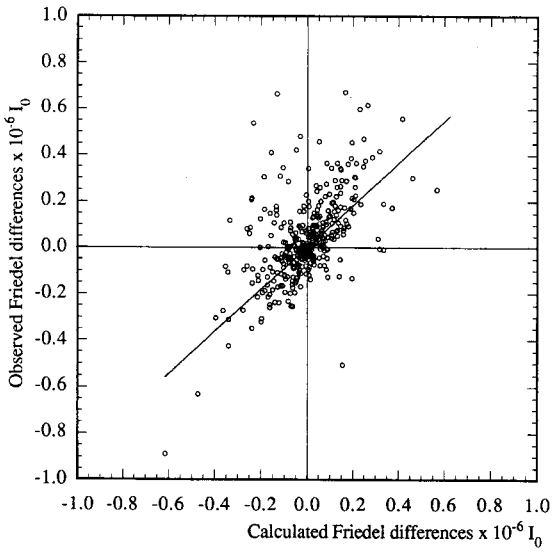

Fig. 1. Plot of calculated and observed Friedel differences for film 746 (I_0 is the intensity of the incident beam). The distribution of data points is anisotropic and elongated along the line also shown in the plot. The line represents a linear fit to the data points (see Section 2) and has a slope of 0.91 indicating a positive correlation between observed and calculated Friedel differences (c.f. Table 2).

Table 2
Correlation coefficients r and standard deviations σ_r (in parentheses) between observed and calculated Friedel differences for diffraction data from untilted and tilted samples at 3.5 Å. For each film there were about 400 Friedel differences to compare. Dynamical calculations were carried out using both the refined atomic model for bR and the experimental density map. The last three columns show results assuming kinematical scattering where Friedel differences are caused by the Ewald sphere curvature only. In each case the R-factor between measured and calculated intensities as well as the average ratio (coefficient b in the linear fit, Eq. (4) in Section 2) of observed to calculated Friedel differences with standard deviation σ_b in parentheses are given

Film	Crystal tilt angle	Dynamical calculation using the atomic model			Dynamical calculation using the map			Kinematical calculation using the map		
	(deg)	r (σ_r)	R	ratio (σ_b)	r (σ_r)	R	ratio (σ_b)	r (σ_r)	R	ratio (σ_b)
551	14.1	0.36 (0.04)	0.26	0.55 (0.07)	0.62 (0.03)	0.11	1.05 (0.07)	0.40 (0.04)	0.11	1.13 (0.13)
552	14.3	−0.35 (0.04)	0.27	−0.52 (0.07)	−0.59 (0.03)	0.11	−0.87 (0.06)	−0.34 (0.04)	0.11	−1.01 (0.14)
560	15.7	0.07 (0.05)	0.26	0.06 (0.08)	0.45 (0.04)	0.12	0.83 (0.08)	0.29 (0.05)	0.12	0.77 (0.12)
746	1.4	0.37 (0.04)	0.26	0.47 (0.06)	0.60 (0.03)	0.09	0.91 (0.06)	0.41 (0.04)	0.09	0.95 (0.14)
857	0.5	−0.41 (0.04)	0.23	−0.44 (0.05)	−0.57 (0.03)	0.07	−0.74 (0.05)	−0.42 (0.04)	0.07	−0.90 (0.12)
858	1.0	−0.37 (0.04)	0.22	−0.42 (0.05)	−0.62 (0.03)	0.09	−0.88 (0.06)	−0.29 (0.05)	0.09	−0.65 (0.13)

Since the density from the atomic model was scaled in the same way as the experimental map, it is likely that the lower ratios are due to inaccuracies in the form factors, the atomic model coordinates or the atomic temperature factors.

Calculations assuming kinematical scattering and Ewald sphere curvature yielded correlation coefficients which were 50% to 70% of those found when dynamical effects where included (cf. last three columns in Table 2). As expected, the contribution from the Ewald sphere curvature to the Friedel differences increases at higher resolution relative to that from dynamical scattering. Fig. 2 shows how the correlation coefficient for one particular film changes with resolution, both with and without dynamical effects included. The correlation coefficient remains well above over the entire resolution range for the dynamical calculation whereas it falls below σ_r at about 9 Å in the kinematical case. The large negative kinematical correlation at very low resolution is not significant as only a small number of measurements were included at that resolution. To see how Friedel differences caused by the Ewald sphere curvature correlate with those due to dynamical scattering, further calculations were carried out where the calculated kinematical Friedel differences were subtracted from the calculated dynamical differences. The remaining Friedel differences in the dynamical calculation were then correlated with the kinematical differences, and it was found that the correlation coefficient dropped below $2\sigma_r$, suggesting the two effects are uncorrelated. This is precisely what would be expected since the kinematical differences depend on very local gradients in the transform of the crystal whereas the dynamical effects result from interference of widely spaced Fourier components of the transform.

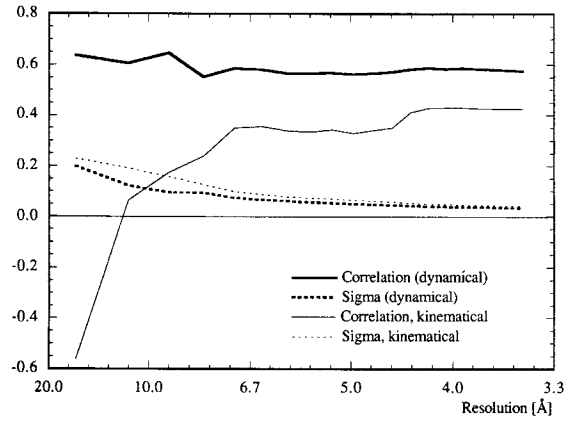

Fig. 2. Dynamical and kinematical correlation in resolution zones for film 857. The correlation between observed and calculated Friedel differences for film 857 is negative (c.f. Table 2). However, to have direct comparison of correlation coefficients and σ_r, the negative of the correlation coefficients for both the dynamical and kinematical calculations were plotted.

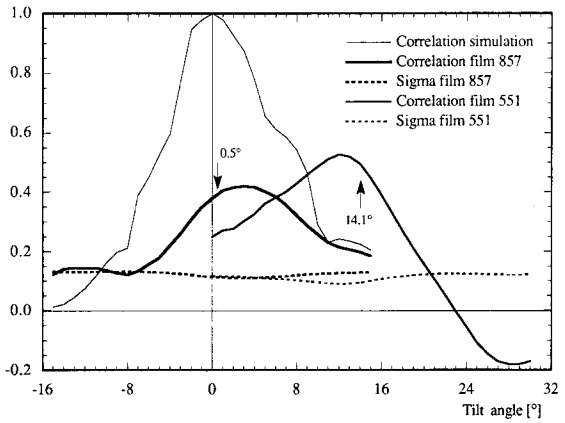

Fig. 3. Exploration of sensitivity of calculations to crystal tilt, showing the correlation coefficient as a function of specimen tilt angle in the dynamical calculation. Correlation coefficients and estimated standard deviations were calculated for an untilted simulated diffraction pattern, for film 551 and for film 857. The nominal tilt angles for film 551 (14.1° tilt) and film 857 (0.5° tilt) are indicated by arrows.

Finally, as a further verification of the results presented here, Fig. 3 shows how the correlation coefficient changes when the specimen tilt and the orientation assumed in the calculation deviate by a small angle. A series of correlation coefficients was calculated between a particular set of data and dynamical calculations using different tilt angles. This was done for experimental diffraction patterns from an untilted specimen and a 14° tilted specimen, and a simulation with the specimen at 0° tilt. The data used in each series were restricted to 8 Å resolution to allow the calculation to be completed within reasonable time. In each case the maximum correlation coincides with the specimen tilt within 2° to 3° and drops below σ_r at an angular deviation of about 8°. The differences in correlation peak positions and nominal tilt angles in Fig. 3 are mainly due to the restricted resolution of the data in the calculation.

The restricted resolution implies the exclusion of beams in the dynamical calculation and causes an error in the calculated intensities and Friedel differences. With higher resolution data, the drop in correlation with angle is sharper. Therefore, the high correlation coefficients actually obtained also imply close agreement between experimental specimen tilt angles and tilt angles assumed in the calculations.

It is worth noting that weak reflections are affected more strongly by dynamical scattering than strong ones, and that the average intensity of a Friedel pair in a dynamical calculation matches closely its kinematical value. The former was also found by Glaeser and Ceska [4] whereas the latter was described earlier by Glaeser and Downing [5].

An interesting and important implication of the work presented here is the possibility to measure and refine structure factor phases as suggested, for example, by Shen and Colella [17]. The calculated differences in intensities of Friedel-related reflections depend on the amplitudes and phases used to calculate the density map. On the other hand, the experimentally observed Friedel-differences can be used as additional independent measurements to determine the density map. For example, to refine structure factor phases, an initial density map could be calculated with existing amplitudes and phases. A correlation coefficient between observed Friedel differences and Friedel differences calculated using the density map could then be evaluated, and incremental changes to the phases could then be made to increase the correlation. In the next refinement cycle a new density map could be calculated with the improved phases. To show that this is possible, but without a full-scale implementation which would require a much greater investment of effort, a series of experimental density maps was calculated where the phase of reflection (4, 3, 0) was altered in steps of 20°. Each new density map was then used to calculate a dynamical diffraction pattern and the Friedel differences were correlated with those measured for a particular film. The result is shown in Fig. 4. Each calculation was again restricted in resolution to 8 Å to be completed within reasonable time. Fig. 4 shows that a phase change of 40° produces a large change in the correlation coefficient. The maximum correlation does not exactly coincide with the calculation using the original phase. This deviation is mainly due to the limited resolution of the calculation which reduces the accuracy of the calculation in a similar way to that affecting the results in Fig. 3. With higher resolution data, the drop in correlation with the phase change is sharper and the phase can be determined more accurately. Changing the phase of a weaker reflection will produce a smaller effect, but it should still be significant when higher resolution data is included.

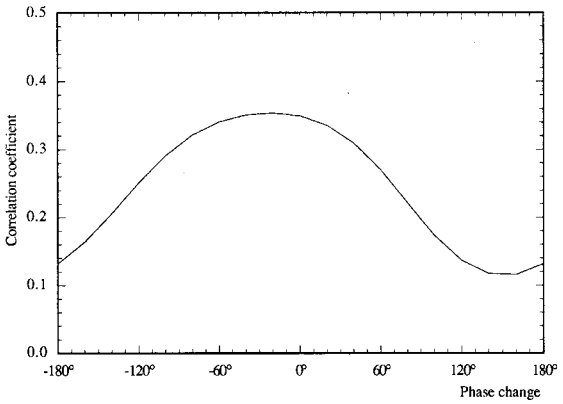

Fig. 4. Correlation between observed Friedel differences on film 746 and calculated differences, as a function of phase change in reflection (4, 3, 0). At the point of 0° phase change the original experimental map was used.

4. Conclusions

The results presented here confirm the earlier hypothesis that the observed differences in intensities of Friedel-related reflections at a resolution of 8 Å and below are mainly due to dynamical scattering. At higher resolution the observed intensity differences in Friedel-related reflections are caused by dynamical scattering as well as the Ewald sphere curvature. Using accurate measurements of these differences it should be possible in future to refine structure factor phases to improve those obtained from electron microscopy.

References

[1] D.M. Bird and M. Saunders, Acta Cryst. A 48 (1992) 555.
[2] R. Henderson, J.M. Baldwin, T.A. Ceska, F. Zemlin, E. Beckmann and K.H. Downing, J. Mol. Biol. 213 (1990) 899.

[3] N. Grigorieff, T.A. Ceska, K.H. Downing, J.M. Baldwin and R. Henderson, J. Mol. Biol., in press (1996).
[4] R.M. Glaeser and T.A. Ceska, Acta Cryst. A 45 (1989) 620.
[5] R.M. Glaeser and K.H. Downing, Ultramicroscopy 52 (1993) 478.
[6] T.A. Ceska and R. Henderson, J. Mol. Biol. 213 (1990) 539.
[7] J.M. Cowley and A.F. Moodie, Acta Cryst. 10 (1957) 609.
[8] J.M. Baldwin and R. Henderson, Ultramicroscopy 14 (1984) 319.
[9] N. Grigorieff and R. Henderson, Ultramicroscopy, in press (1995).
[10] P. Goodman and A.F. Moodie, Acta Cryst. A 30 (1974) 280.
[11] D.M. Bird, Acta Cryst. A 46 (1990) 208.
[12] P.B. Hirsch, A. Howie, R.B. Nicholson, D.W. Pachley and M.J. Whelan, Electron microscopy of thin crystals (Butterworths, London, 1965).
[13] J.M. Cowley, Diffraction physics (North-Holland, Amsterdam, 1975).
[14] J.M. Cowley, in: International Tables for Crystallography, ed. A.J.C. Wilson (Kluwer Academic Publishers, Dordrecht, 1992) p. 223.
[15] L.S. Bartell, in: Stereochemical applications of gas-phase electron diffraction, eds. I. Hargittai and M. Hargittai (VCH, Weinheim, 1988) p. 55.
[16] S. Konaka, in: Stereochemical applications of gas-phase electron diffraction, eds. I. Hargittai and M. Hargittai (VCH, Weinheim, 1988) p. 85.
[17] W. Shen and R. Colella, Nature 329 (1987) 232.